Differential geometric approach to atmospheric refraction

William C. Kropla and Waldemar H. Lehn

Department of Electrical Engineering, University of Manitoba, Winnipeg, Manitoba R3T 2N2, Canada

Received March 4, 1991; revised manuscript received October 28, 1991; accepted October 29, 1991

Differential geometric techniques are presented and used to model the optical properties of the atmosphere under conditions that produce superior mirages. Optical path length replaces the usual Euclidean metric as a distance-measuring function and is used to construct a surface on which the paths of light rays are geodesics. The geodesic equations are shown to be equivalent to the ray equation in the plane. A differential equation that relates the Gaussian curvature of the surface and the refractive index of the atmosphere is derived. This equation is solved for the cases in which the curvature vanishes or is constant. Illustrative examples based on observation demonstrate the use of geometric techniques in the analysis of mirage images.

INTRODUCTION

Mirages are the images that result when the atmosphere refracts light rays away from their usual (nearly straight) paths. Sufficiently large temperature gradients will cause changes to the curvature of ray paths large enough to give rise to images that are elevated or depressed with respect to the actual object. These images are called, respectively, superior and inferior mirages. The former arise from a temperature inversion, the latter from the more usual decrease of temperature with elevation.

Pernter and Exner[1] carried out an early classification of mirages. They identified atmospheres that produced certain simple shapes of ray paths and roughly classified the properties of observed mirages. To summarize briefly the relevant results: Linear variation of refractive index n with height produces parabolic ray paths, while quadratic variation produces circular paths. The nature of the variation determines the mirage images observed. In the linear case the image is elevated or depressed but undistorted. If n decreases nonlinearly with height (such that its gradient has maximum magnitude at the surface), an elevated mirage, consisting of a single distorted image, is seen. If the refractive-index (or temperature) profile contains a point of inflection, it produces the classic three-image mirage with alternating erect and inverted images, as was observed by Vince in 1798.[2] This form also produces optical ducting conditions, as identified by Lehn and Schroeder,[3] in which light rays are trapped beneath the inversion (found at the inflection point elevation) for long distances.

The present paper extends the mirage classification process: It presents ray path forms for atmospheres with certain properties, and it discusses the resulting imaging. In the following sections we present some techniques of differential geometry[4] that were not previously applied to the study of mirages. Specifically, we endow the Euclidean plane with a new metric structure, the optical path length. The surface that results is, in some ways, a more natural home for optical problems since the paths of light rays will be geodesics on this surface. We will derive the ray equation from the specified metric function and present the results of modeling the atmosphere by a surface whose Gaussian curvature vanishes or is constant. We show that so constraining the Gaussian curvature produces a class of temperature profiles that are typical of many observed mirages.

DIFFERENTIAL GEOMETRY

The path followed by a ray of light in an atmosphere of constant refractive index is a straight line. The straight line constitutes a geodesic, or a distance-extremizing curve, in the Euclidean plane. The path followed by a ray in a laterally homogeneous atmosphere with a nonconstant vertical refractive profile is a plane curve. By Fermat's principle the time of travel along the ray will be less than the time of travel along all the nearby paths. It follows that the optical path length between two points on the ray will also be minimized. Clearly, the curved path is not a geodesic in the plane. We can, however, define a surface wherein all the paths of light rays are geodesics by replacing the Euclidean metric of the plane and by using the optical path length to measure distance.[5]

If we restrict our attention to a ray that travels in the x–z plane, then, for arbitrarily close points on the ray, the optical path length is $\mathrm{d}l = n(x,z)\mathrm{d}s$, where $\mathrm{d}s^2 = \mathrm{d}x^2 + \mathrm{d}z^2$ and n is the refractive index. The line element $\mathrm{d}s$ lies in the Euclidean plane, and $\mathrm{d}l$ is the line element on a two-dimensional surface, M, that is defined (at least locally) by this relation. If we identify x^1 with x and x^2 with z, then, since $\mathrm{d}l^2 = n^2(\mathrm{d}x^2 + \mathrm{d}z^2) = n^2\delta_{ij}\mathrm{d}x^i\mathrm{d}x^j = g_{ij}\mathrm{d}x^i\mathrm{d}x^j$ and assuming that n is a function of elevation alone, the covariant metric tensor and its contravariant counterpart are

$$g_{ij} = n^2(z)\delta_{ij},$$

$$g^{ij} = \frac{1}{n^2}\delta^{ij}, \tag{1}$$

where use of the summation convention is made. (See Appendix A for a fuller exposition of the geometry and the tensor analysis used here.) Associated with this metric are the nonvanishing Christoffel symbols of the second kind,

$$-\Gamma_1{}^2{}_1 = \Gamma_2{}^2{}_2 = \Gamma_1{}^1{}_2 = \Gamma_2{}^1{}_1 = \frac{1}{n}\frac{\mathrm{d}n}{\mathrm{d}z}. \tag{2}$$

0740-3232/92/040601-08$05.00 © 1992 Optical Society of America

The parametric equation describing a geodesic on a surface is

$$\frac{d^2x^i}{dl^2} + \Gamma^i_{j\,k}\frac{dx^j}{dl}\frac{dx^k}{dl} = 0, \tag{3}$$

where the indices i, j, and k take on values of 1 and 2. Substituting the Christoffel symbols from Eq. (2) into Eq. (3), we obtain a pair of parametric equations, with parameter l, describing the geodesics of the surface M,

$$\frac{d^2x}{dl^2} + \frac{2}{n}\frac{dn}{dz}\frac{dx}{dl}\frac{dz}{dl} = 0,$$

$$\frac{d^2z}{dl^2} + \frac{1}{n}\frac{dn}{dz}\left[\left(\frac{dz}{dl}\right)^2 - \left(\frac{dx}{dl}\right)^2\right] = 0. \tag{4}$$

We have defined the line element on M so that $dl = n\,ds$. The chain rule allows us to write

$$\frac{dx}{dl} = \frac{dx}{ds}\frac{ds}{dl} = \frac{1}{n}\frac{dx}{ds},$$

$$\frac{dz}{dl} = \frac{dz}{ds}\frac{ds}{dl} = \frac{1}{n}\frac{dz}{ds}, \tag{5}$$

$$\frac{d^2x}{dl^2} = \frac{1}{n^2}\frac{d^2x}{ds^2} + \frac{1}{n}\frac{d}{dz}\left(\frac{1}{n}\frac{dx}{ds}\frac{dz}{ds}\right),$$

$$\frac{d^2z}{dl^2} = \frac{1}{n^2}\frac{d^2z}{ds^2} + \frac{1}{n}\frac{d}{dz}\left(\frac{1}{n}\frac{dz}{ds}\frac{dz}{ds}\right), \tag{6}$$

which, on substitution in Eqs. (4), yield a standard result, the vector form of the ray equation

$$\frac{d}{ds}\left(n\frac{d\mathbf{r}}{ds}\right) = \nabla n, \tag{7}$$

where $\mathbf{r}$ locates a point on the ray in the x–z plane.

It can be shown[6] that the Gaussian curvature K of a surface is given by

$$K = \frac{R_{1212}}{|g|}, \tag{8}$$

where R_{1212} is the [1212] component of the covariant curvature tensor and $|g|$ is the determinant of the metric tensor, treated as a matrix (see Appendix A). Performing the calculations implicit in Eq. (8), we obtain a second-order, nonlinear differential equation relating the refractive index and the Gaussian curvature,

$$\frac{d^2n}{dz^2} - \frac{1}{n}\left(\frac{dn}{dz}\right)^2 = -n^3K. \tag{9}$$

Before we proceed to examine the solutions of this equation for zero and for constant K, it is useful to obtain an explicit relation between the refractive index and the temperature, since temperature is much easier to measure.

We use the relation[7]

$$n = 1 + \epsilon\rho = 1 + \frac{\epsilon\beta p}{T}, \tag{10}$$

where ρ is the density, p is the pressure, T is the absolute temperature, ϵ is the specific polarizability of air (226×10^{-6} m^3 kg^{-1}), and β is the reciprocal of the specific gas constant for dry air (3.48×10^{-3} kg K J^{-1}), to convert from the refractive to the temperature profile. Since n is always near unity, it is more convenient to use refractivity $r = n - 1$ in the development. An explicit equation for temperature in terms of refractivity is obtained as follows. Rewrite Eq. (10) as

$$rT = \epsilon\beta p, \tag{11}$$

where r, T, and p are all functions of elevation z. Differentiation of Eq. (11) with respect to z permits the elimination of ρ, since $dp/dz = -\rho g$ for an atmosphere in a gravitational field g. Thus

$$\frac{d(rT)}{dz} = -\beta g(\epsilon\rho) = -\beta g r, \tag{12}$$

which integrates to

$$T(z) = \frac{1}{r(z)}\left[r_0T_0 - \beta g\int_0^z r(z')dz'\right]. \tag{13}$$

VANISHING GAUSSIAN CURVATURE

The solution of Eq. (9) for $K = 0$ is $n = ae^{bz}$, where a and b are constants of integration. When this exponential is substituted into Eq. (13) we obtain the exact temperature profile that corresponds to $K = 0$:

$$T(z) = \frac{1}{a\exp(bz) - 1}\left\{r_0T_0 - \frac{\beta g a}{b}[\exp(bz) - 1] + \beta g z\right\}. \tag{14}$$

If the refractive index is known at two points, $z = 0$ and $z = z_e$, then

$$a = n_0 = r_0 + 1, \tag{15}$$

$$b = \frac{1}{z_e}\ln\frac{n_e}{n_0} = \frac{1}{z_e}\ln\left(\frac{1 + r_e}{1 + r_0}\right). \tag{16}$$

Since the refractivity of air is small, Eq. (16) can be approximated quite accurately by

$$b \simeq \frac{r_e - r_0}{z_e} = \frac{n_e - n_0}{z_e}. \tag{17}$$

This shows that b is also small, a fact that permits us to expand the exponentials in Eq. (14) in a short power series. Expand the denominator exponential to the quadratic term, and bring these terms into the numerator, using the series for $1/(1 + \delta)$, again to the quadratic term. After expanding the numerator exponential (to the linear term), multiply everything out and truncate after the quadratic term to get

$$T(z) = T_0 + z\left(-\beta g - \frac{abT_0}{r_0}\right) + z^2\left[\frac{\beta g a b}{r_0} - \frac{ab^2T_0}{r_0}\left(\frac{1}{2} - \frac{a}{r_0}\right)\right], \tag{18}$$

which agrees with Eq. (14) to better than 0.1° for temperature gradients as high as 0.2 K m^{-1} and elevations as high as 50 m.

Our objective, however, was to show that $T(z)$ is predominantly linear. This becomes clear when some typical numbers are inserted. Let $T_0 = 273$ K and $p_0 = 1.0133 \times 10^5$ Pa. Then $r_0 = 291.92 \times 10^{-6}$. If the linear term is taken to be the (fairly strong) gradient of 0.2 K m^{-1}, then $b = -250.3 \times 10^{-9}$ m^{-1}. For these values the quadratic term has the coefficient 1.715×10^{-4} K m^{-2}. Thus the linear term dominates at low elevations. At 25 m the difference between Eq. (14) and the linear version of Eq. (18) is 0.12°.

For atmospheres in which the refractive index is a function of z only (or, in a spherical system, a function of the radial distance only), it is easy to show[8] that the Euclidean ray curvature κ is given by

$$\kappa = -\frac{\sin\theta}{n}\frac{dn}{dz}, \tag{19}$$

where θ is the zenith angle of the tangent to the ray. When the exponential solution corresponding to zero Gaussian curvature is used here, we obtain

$$\kappa = -b \sin\theta \simeq -b, \tag{20}$$

since in practical mirage situations θ is close to 90°.

The visual effect of mirages with a vanishing curvature is simple and often not perceived: Images are vertically displaced, with unit magnification.[1] The most obvious example is the normal well-mixed atmosphere in which the temperature gradient is -0.006 K m^{-1}; we usually ignore the slight vertical displacement and see everything to the correct scale. More interesting is the temperature inversion; for example, with $T_0 = 273$ K and a gradient of $+0.112$ K m^{-1}, horizontal rays have the same curvature as the Earth. Objects maintain their normal appearance and scale, but the Earth then appears to be flat.

The imaging properties of the atmosphere at a given object distance are conveniently presented on a graph where the apparent elevations of the object points are plotted against their actual elevations. This curve has been variously named the transfer characteristic[9] (TC), the transfer mapping,[10] and the image diagram.[11] Its slope is the image magnification. In the hypothetical case of straight rays on a flat Earth, the TC would be a straight line of unit slope passing through the origin. On a curved Earth straight rays produce an offset TC, which intersects the abscissa at a value given by the departure of the Earth's shape from flatness at the object distance. For mirages with vanishing Gaussian curvature, the TC remains straight with unit slope but gains additional offset.

In summary, a vanishing Gaussian curvature implies an exponential variation of the refractive index with elevation (exactly) and a linear variation of temperature (approximately); and all nearly horizontal rays have the same Euclidean curvature.

CONSTANT GAUSSIAN CURVATURE

Solving Eq. (9) for the case of K = constant, we obtain

$$n = \frac{2ac}{\sqrt{K}}\frac{\exp(-az)}{\exp(-2az) + c^2}, \tag{21}$$

where a and c are the constants of integration. The negative sign in the exponentials is the result of assuming that the refractive index decreases with elevation, i.e., that the temperature increases with elevation. It is under these conditions of temperature inversion that a superior mirage may be observed. If we again use n_0 for the refractive index at $z = 0$ we can rewrite Eq. (21) as

$$n(z) = n_0(1 + c^2)\frac{\exp(-az)}{\exp(-2az) + c^2}, \tag{22}$$

with

$$a = n_0\sqrt{K}\,\frac{1 + c^2}{2c}. \tag{23}$$

Interpretation is facilitated if we use Eq. (22) to express the refractivity $r(z) = n - 1$ and then apply power-series expansions. Numerical testing with practical temperature profiles indicates that a and K are small and that c is near unity. If $c = 1$ identically, then Eq. (22) can be written as $n = n_0\,\mathrm{sech}(az)$. In the more general case, we replace each exponential by a quadratic power series; then the denominator series, when written in the form $1 + \delta$, can be brought into the numerator. When the resulting expression is expanded as a power series in z and truncated after the quadratic term, the result is

$$r(z) = r_0 + n_0^2\sqrt{K}\,\frac{1 - c^2}{2c}z + n_0^3K\frac{1 - 6c^2 + c^4}{8c^2}z^2, \tag{24}$$

with $n_0 = r_0 + 1$ as before and $r_0 = \epsilon\beta p_0/T_0$ from Eq. (11). This may be further simplified if c is replaced by $1 + \gamma$, where γ is small. Neglecting the terms in γ^2, we obtain

$$r(z) = r_0 - n_0^2\gamma\sqrt{K}\,z - \frac{n_0^3K}{2}z^2, \tag{25}$$

with

$$a = n_0\sqrt{K}\,. \tag{26}$$

Equation (13) can be integrated in closed form if Eq. (25) is substituted into it. The result consists of a cubic polynomial divided by the quadratic $r(z)$ function. When the denominator is brought into the numerator (by series) and the result is truncated at the quadratic term, we obtain

$$T(z) = T_0 + b_1z + b_2z^2, \tag{27}$$

where

$$b_1 = \frac{n_0^2\gamma T_0\sqrt{K}}{r_0} - g\beta, \tag{28}$$

$$b_2 = \frac{n_0^3T_0K}{2r_0} \tag{29}$$

(in b_2, relatively small terms have again been dropped). Equation (29) permits an interesting interpretation: The quadratic coefficient b_2 is directly proportional to the Gaussian curvature.

In the examples that follow, it is shown that, for practical inversion profiles, these series approximations with their assumptions on the smallness of certain parameters are justified.

If measurements or calculations provide a quadratic temperature profile, then T_0, b_1, b_2 are known, and the

Table 1. Temperature (T) Profiles for Examples A and B

Profile 1		Profile 2	
z (m)	T (°C)	z (m)	T (°C)
0.0	−1.90	0.0	−32.00
1.2	−1.88	10.0	−32.00
3.2	−1.82	20.0	−31.90
5.2	−1.69	30.0	−31.40
8.0	−1.32	40.0	−30.45
9.6	−0.93	50.0	−29.40
11.2	−0.37	65.0	−27.65
12.8	0.55	75.0	−26.70
13.6	1.27	85.0	−26.00
14.0	1.65	95.0	−25.40

above equations are easily inverted to give a, γ, and K:

$$a = \left(\frac{2b_2 r_0}{n_0 T_0}\right)^{1/2}, \tag{30}$$

$$\gamma = \frac{r_0(b_1 + g\beta)}{a n_0 T_0}, \tag{31}$$

$$K = \frac{a^2}{{n_0}^2}. \tag{32}$$

The parabolic temperature profile of Eq. (27) produces a linear TC; this is consistent with the study of Rees,[11] in which the assumption of a linear image diagram leads to a parabolic refractive profile. A linear TC produces a clear image whose only distortion is a vertical magnification (of a magnitude strictly greater than unity). If the image is inverted, then the sign of the magnification is negative. If portions of actual mirages possess these properties we can attempt to model portions of the temperature profile by assuming a constant K.

The assumption of a constant, positive Gaussian curvature implies that the surface that we are using to model the plane of the ray path is a segment of a sphere of radius $R = 1/\sqrt{K}$. All the geodesics through a point on such a surface will intersect at the antipodal point. This focusing effect is evident in all the ray traces generated from Eq. (22) (see Fig. 2 below).

EXAMPLES

In each of the following examples temperature T is in kelvins and elevation z is measured in meters above sea level.

(A) One of the profiles used to reproduce an observed Novaya Zemlya effect[12] is a suitable candidate. This profile (profile 1; Table 1) creates an optical duct that traps nearly horizontal rays between the ground and an elevation of 9.6 m. Over this range the profile looks nearly parabolic; a least-squares fit produces

$$T(z) = 271.12 - 0.0316z + 0.0133z^2. \tag{33}$$

Figure 1(a) shows the original and the parabolic fit, which follows the original to within 0.05° over the range of interest. Because $T(z)$ generates basically the same ray paths as profile 1, the fit can be considered good. This is the most significant comparison criterion, for it means that the images observed will be similar. The corresponding values of a, γ, and K, as calculated from Eqs. (30)–(32) using the previously given values for ϵ, β, and p_0, are given in Table 2. The ray paths for $T(z)$ are shown in Fig. 2, where the focusing at the antipodal points of the spherical modeling surface is evident. The distance between focal points is given by $D = \pi/\sqrt{K}$.

The smallness of the parameters a, γ, and K justifies the series-expansion approximations made in the derivations. The accuracy has also been verified by substituting these values into the exponential solution [Eq. (21)] and integrating it according to Eq. (13) to find the exact temperature profile for these parameters. The difference between this and Eq. (33) is less than 0.01° over the range of interest.

The quadratic refractivity equation for this profile is

$$r(z) = 293.8 \times 10^{-6} - (2.749 \times 10^{-9})z - (14.40 \times 10^{-9})z^2. \tag{34}$$

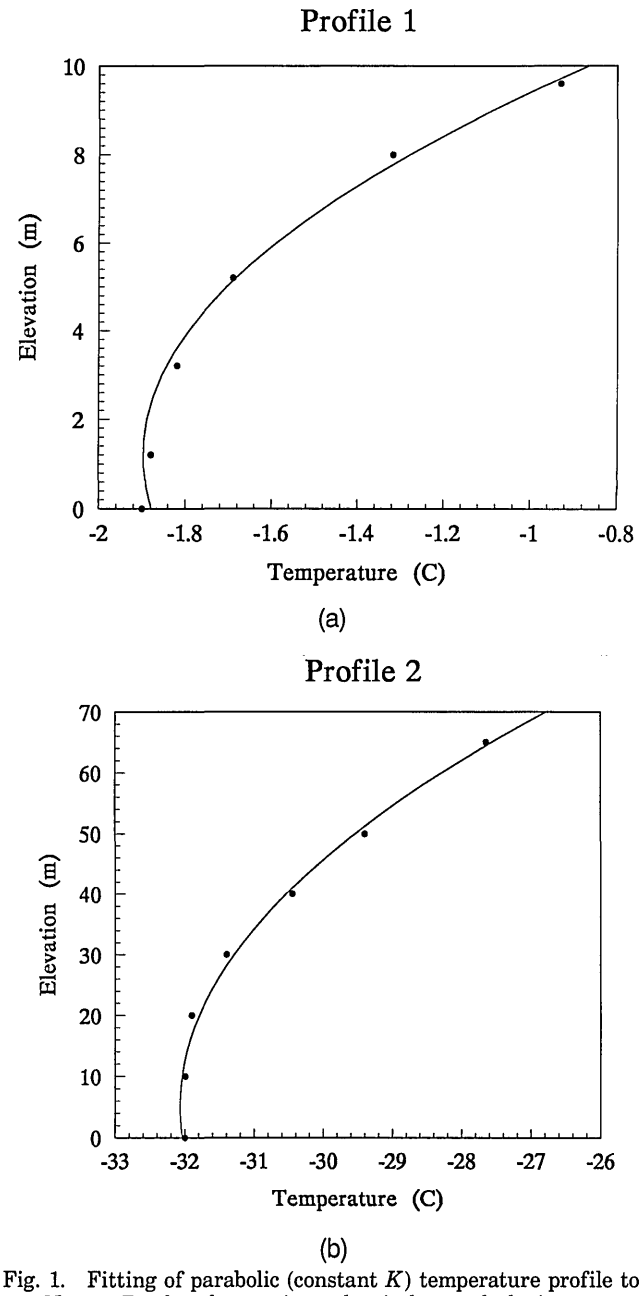

Fig. 1. Fitting of parabolic (constant K) temperature profile to two Novaya Zemlya observations; the circles mark the input temperatures, and the solid curves show the parabolic fit.

Table 2. Parameter Values for Profiles 1 and 2

Parameter	Profile 1	Profile 2
a (m^{-1})	169.7×10^{-6}	58.63×10^{-6}
γ	16.20×10^{-6}	500.7×10^{-6}
K (m^{-2})	28.78×10^{-9}	3.435×10^{-9}

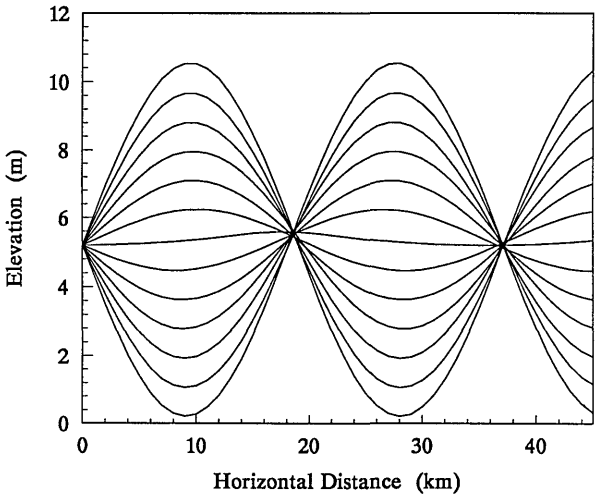

Fig. 2. Calculated ray paths derived from profile 1, exhibiting strong focusing at the antipodal points of the spherical modeling surface.

While the linear and the quadratic terms have coefficients that are quite small in relation to r_0, they cannot be neglected. The function is clearly parabolic and must be so to generate the parabolic $T(z)$. Changing the shape of r (perhaps by claiming that over such a small range almost any function can be fitted to the data) changes the shape of $T(z)$, the nature of the ray paths, and the nature of the images produced. The imaging properties are a sensitive function of the temperature and hence of $r(z)$.

(B) The basis for the second example is a Novaya Zemlya effect observed in 1951.[13] Profile 2 (Table 1) was calculated to reproduce the observation[14]; the corresponding light rays travel within an optical duct of height 65 m over a distance of approximately 400 km. The portion of the temperature profile that defines the duct is approximated to within 0.1° by a least-squares parabolic fit:

$$T(z) = 240.96 - 0.01272z + 0.001254z^2. \quad (35)$$

Figure 1(b) compares the original with the parabola; they produce ray paths with similar properties. Table 2 shows the resulting values of a, γ, K. Again, the parameters are suitably small for the series expansions. The relevant expression for refractivity is

$$r(z) = 330.5 \times 10^{-6} - (29.36 \times 10^{-9})z - (1.719 \times 10^{-9})z^2. \quad (36)$$

When this is substituted into the exact equation for temperature, the maximum difference between that equation and Eq. (35) is ~0.15°.

(C) In other cases portions of profiles may be modeled. Figure 3(a) shows an unusually clear and well-defined superior mirage observed at Tuktoyaktuk, Northwest Territories, Canada, on May 16, 1979. The line of sight, 20 km long, passed over the frozen Beaufort Sea from a camera elevation of 2.5 m. The target was Whitefish Summit, 20.3 m high,[15] shown in undistorted form in Fig. 3(b). A comparison of the two images permits the construction of the partial TC shown by the heavy lines in Fig. 4. Gaps are present in this TC because of a lack of elevation information for those rays producing sky images. Any synthesized TC that coincides with the measured partial TC will produce the same mirage of the summit.

The TC partitions naturally into three zones. In zone I we have an undistorted erect image whose magnification of 1.04 is close to unity. For straight rays the expected TC offset at 20 km would be 31.4 m. Because the observed TC has a (projected) offset of only 8.1 m, the image has been vertically displaced (raised). Unit magnification and vertical displacement are the properties of zero Gaussian curvature, which implies a linear temperature profile. Hence zone I will be so modeled.

In zone II we again have a linear TC but this time with a magnification of −1.33. This suggests a constant K and a parabolic temperature profile. This zone will thus be modeled as a parabolic function smoothly attached to the linear profile of zone I.

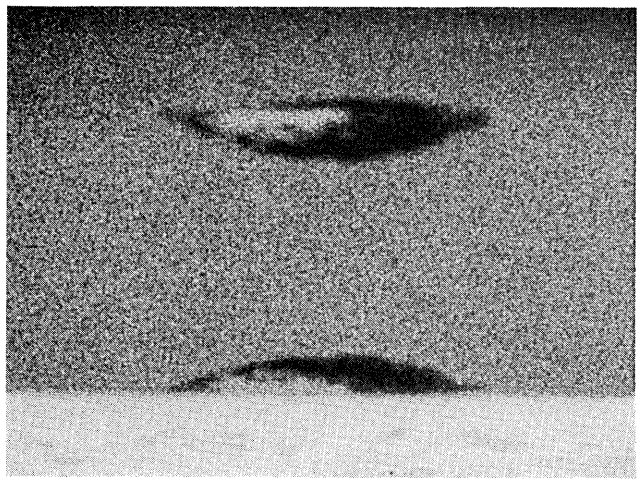

(a)

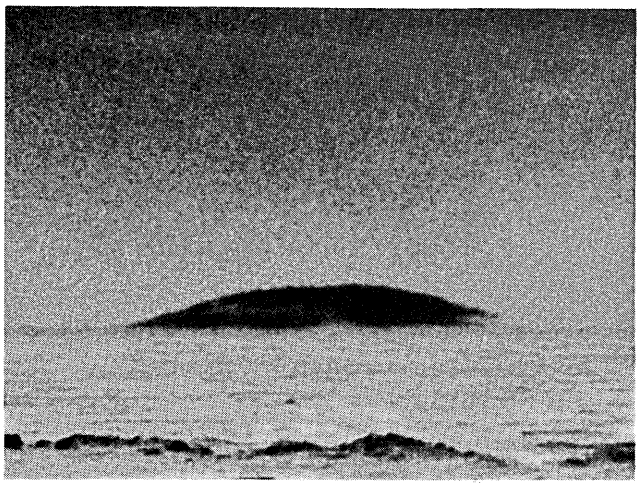

(b)

Fig. 3. Whitefish Summit photographed with a 560-mm lens from Tuktoyaktuk, Northwest Territories, Canada, over a range of 20 km. (a) Superior mirage: May 16, 1979, 03.12 mountain daylight time, camera elevation 2.5 m. (b) Normal view: camera elevation 5.8 m.

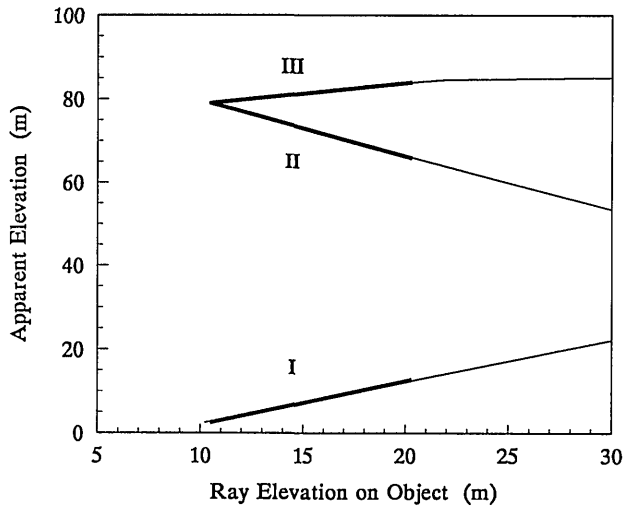

Fig. 4. TC's: heavy lines, observed; thin lines, calculated. Zones I–III are described in the text.

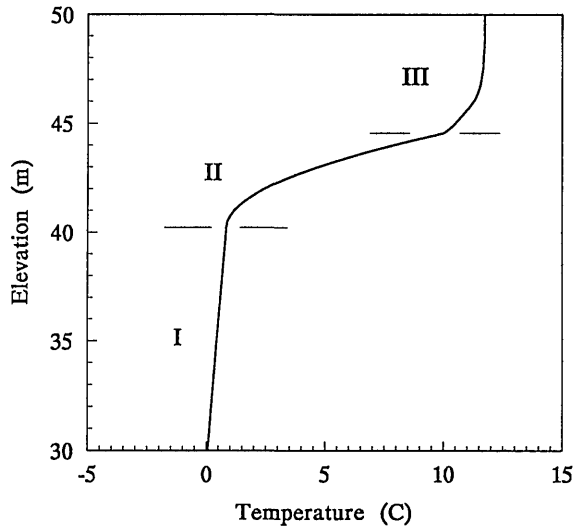

Fig. 5. Temperature profile that generates the fitted TC of Fig. 4. Zones I–III are described in the text.

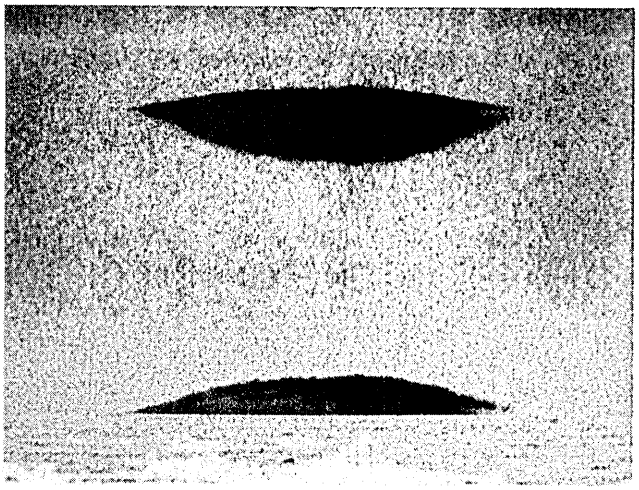

Fig. 6. Calculated mirage image based on the calculated TC.

Once this simple model is constructed, finding the parameters to produce the correct TC is easily done by using a ray-tracing program. Starting with zone I, with the eye-level temperature fixed at 271 K, the temperature gradient is varied until an exact match with the TC is found. This occurs at a gradient of 0.075 K m^{-1}. The linear temperature profile is extended upward and capped with a constant K profile. In zone II we have two adjustable parameters available to us: K and the transition elevation of the bottom of zone II. The value of γ is not adjustable but is determined by the smoothness constraint. Recall from Eq. (29) that K is proportional to the quadratic coefficient of the parabolic temperature profile. K controls the slope (magnification) of the resulting TC, so K is adjusted until a match to the zone II slope is found; then the elevation is adjusted until the computed TC coincides with the observed TC. A good fit is produced when $K = 0.994 \times 10^{-6}$ m^{-2}, with a transition elevation of 40.22 m. The temperature profile itself is

$$T(y) = 273.825 + 0.075y + 0.471y^2, \tag{37}$$

where $y = z - 40.22$.

Zone III was more problematic, and we suspect that specifying the Gaussian curvature here is not an effective way to model the refractive profile, since the rays that reach this level have done so after traversing both of the lower zones, and any errors in modeling there will propagate upward. We chose, therefore, to model zone III in the manner described below.

In zone III a ray-steering algorithm, developed by Lehn, was adopted. Noting that the rays with an initial elevation angle greater than 13.15 arcmin reach the target at successively higher elevations, we reduced the temperature gradient at points above the vertex of this ray (44.56 m) so that the next ray fell on the desired TC. This procedure was repeated for higher rays to produce all of zone III. The resulting TC and the synthesized temperature profile are shown in Figs. 4 and 5, respectively. The Earth's curvature was implicit in the algorithm that produced the TC.

Figure 6 shows the mirage image calculated from a digitized version of the undistorted photograph. The close agreement between the original and the reconstructed image is evident and indicates that superior mirages can be classified and modeled effectively by differential geometric techniques.

CONCLUSIONS

A new method of describing atmospheric refraction problems has been developed. By the appropriate selection of Gaussian curvature a variety of optical conditions can be modeled. The assumption of a constant, positive Gaussian curvature leads to a closed solution to the differential equation relating the refractive index and the Gaussian curvature. This solution describes a class of superior mirages that exhibit strong focusing.

APPENDIX A: DIFFERENTIAL GEOMETRY

We define an abstract surface in Euclidean three-space as a set of points M in E^3 and a set of mappings (called patches or coordinate neighborhoods) from open sets in the Euclidean plane, E^2, to open sets in M. Every point in M must lie in the image of at least one patch, and where two patches, $\mathbf{x}$ and $\mathbf{y}$, overlap, the composite mappings $\mathbf{y}^{-1}\mathbf{x}$ and $\mathbf{x}^{-1}\mathbf{y}$ must be differentiable. The differentiability condition guarantees the existence of differentiable co-

ordinate transformations where patches overlap, should a surface not be covered by a single patch.

A patch is commonly the way we define a surface algebraically; consider, for example, the patch $\mathbf{x}(u,v) = [u,v,(1-u^2-v^2)^{1/2}]$ for $u,v < 1$, which covers the upper half of the unit sphere except for the points lying on the equator. To cover the entire sphere requires six hemispherical patches: top, bottom, right, left, front, and back.

A geometric surface is an abstract surface endowed with a geometric structure by means of a metric or a distance-measuring function and corresponds to the usual notion of a surface. Strictly speaking, the metric is a consequence of defining an inner product on each of the tangent planes of M, but this notion is not required for the work presented here.

The choice of a metric is not unique. In the plane, viewed as a geometric surface, we have the usual Euclidean metric $ds^2 = dx^2 + dy^2$ in line element form, and on the surface of the unit sphere the metric is given by $ds^2 = d\theta^2 + \sin^2\theta d\phi^2$. By a suitable redefinition of the metric on each of these surfaces, the geometric structures can be interchanged, resulting in the so-called stereographic plane and the stereographic sphere. (See, for example, Ref. 16.)

It is usual in classical tensor analysis to employ the so-called summation convention; that is, when any index occurs as both a superscript and a subscript in an expression there is an implicit summation over that index. We follow this convention below.

The metric of a two-dimensional geometric surface can be expressed as $ds^2 = g_{ij}dx^i dx^j$. Each of the four terms g_{ij} constitutes an element of the metric tensor. In the Euclidean plane $g_{ij} = \delta_{ij}$, the Kronecker delta, while on the surface of the unit sphere and employing spherical polar coordinates

$$g_{ij} = \begin{bmatrix} 1 & 0 \\ 0 & \sin^2\theta \end{bmatrix}.$$

Both of these examples are symmetric, second-rank tensors, and they are, evidently, differentiable. The inverse of the metric tensor is written as g^{ij} and is obtained from g_{ij} by the usual methods of matrix inversion. The metric tensor associated with the unit sphere, expressed with respect to a polar coordinate system, is singular at the pole. It should be clear that this defect arises from the coordinate system chosen and not from any defect of the spherical surface. Practically this means that we work away from the pole or recoordinate the surface as necessary to remove the singularity.

On surfaces that do not admit of a Cartesian coordinate system there is a distinction to be made between contravariant and covariant vectors (or first-rank tensors). Under coordinate transformations, a contravariant vector transforms as a differential, and its components are denoted by superscripts. A covariant vector, on the other hand, transforms as a gradient, and its components are denoted by subscripts. These notions generalize to higher-rank tensors, but specific transformation laws are not required here.

Christoffel symbols of the first kind are defined by the relation

$$\Gamma_{hlk} = \frac{1}{2}\left(\frac{\partial g_{kl}}{\partial x^h} + \frac{\partial g_{lh}}{\partial x^k} - \frac{\partial g_{hk}}{\partial x^l}\right),$$

and Christoffel symbols of the second kind are defined by

$$\Gamma_h{}^j{}_k = g^{lj}\Gamma_{hlk}.$$

We define the absolute differential of the contravariant vector X^j as

$$DX^j = dX^j + \Gamma_h{}^j{}_k X^h dx^k$$

and the absolute differential of the covariant vector Y_h as

$$DY_h = dY_h - \Gamma_h{}^l{}_k Y_l dx^k.$$

In E^3, the tangents of a straight line are all parallel to one another, and the conventional differentials of the components of the tanget vectors vanish. A vector field, $X^j(t)$, along a curve Λ in M is said to be parallel if its absolute differential vanishes along Λ. The components of the tangents of Λ (which form a vector field along the curve) are given by $\dot{x}^j$, where the dot indicates a conventional differentiation with respect to parameter t. Hence the condition that tangents along Λ are parallel can be expressed as

$$D\dot{x}^j = d\dot{x}^j + \Gamma_h{}^j{}_k \dot{x}^h dx^k = 0$$

or

$$\frac{d^2x^j}{dt^2} + \Gamma_h{}^j{}_k \frac{dx^h}{dt}\frac{dx^k}{dt} = 0.$$

These parametric equations define the geodesics of the surface M.

The conventional derivatives of tensor quantities on a geometric surface are, in general, not tensors. We define the covariant derivative of a contravariant vector X^p with respect to x^k:

$$X^p_{|k} = \frac{\partial X^p}{\partial x^k} + \Gamma_h{}^p{}_k X^h$$

and of a covariant vector Y_h with respect to x^k:

$$Y_{h|k} = \frac{\partial Y_h}{\partial x^k} - \Gamma_h{}^m{}_k Y_m.$$

The covariant derivative of any tensor quantity produces a new tensor quantity with the covariant rank increased by one. A necessary condition for the existence of such a covariant derivative is the existence on the surface of a nonsingular, differentiable, symmetric second-rank tensor. The metric tensor will suffice on any region where it is nonsingular. The Christoffel symbols of the second kind, $\Gamma_h{}^p{}_k$, then constitute an affine connection of the surface. A connection is said to be symmetric if $\Gamma_h{}^p{}_k = \Gamma_k{}^p{}_h$.

The conventional partial differentiation of a scalar function is, subject to continuity constraints, symmetric with respect to order, while repeated covariant differentiation is, in general, not. It can be shown that $X^j_{|h|k} - X^j_{|k|h} = 0$ implies that the tensor quantity

$$R_l{}^j{}_{hk} = \frac{\partial \Gamma_l{}^j{}_h}{\partial x^k} - \frac{\partial \Gamma_l{}^j{}_k}{\partial x^h} + \Gamma_m{}^j{}_k \Gamma_l{}^m{}_h - \Gamma_m{}^j{}_h \Gamma_l{}^m{}_k$$

vanishes when calculated with respect to a symmetric connection. $R_l{}^j{}_{hk}$ is referred to as the curvature tensor. If the curvature tensor is nonzero, then clearly we must

distinguish between $X^j_{|h|k}$ and $X^j_{|k|h}$. The curvature tensor is skew symmetric with respect to interchange of the last two covariant indices.

The covariant curvature tensor is defined by the relation $R_{lmhk} = g_{jm}R_l{}^j{}_{hk}$, and some counting will show that on a two-dimensional surface it possesses only one independent component, the [1212] component, all others being zero or $\pm R_{1212}$.

If $\alpha(s)$ is a plane curve parameterized by arc length s, then the curvature $k = k(s)$ of α is defined to be

$$k(s) = \frac{\mathrm{d}\mathbf{t}}{\mathrm{d}s} \cdot \mathbf{n},$$

where $\mathbf{t}$ and $\mathbf{n}$ are the unit tangent and the unit normal, respectively, of α. Intuitively we note that k measures the rate of change of direction of the tangent vector with respect to arc length.

Suppose that we have a two-dimensional surface with a unique (up to sign) normal at every point. The intersection of the surface and a plane containing the normal defines a plane curve, the curvature of which is called the normal curvature of the surface. As this plane rotates about the normal at $\mathbf{p}$, the normal curvature at $\mathbf{p}$ will be given as a function of the rotation angle. If the surface is sufficiently smooth, with no self-intersections, there will be two cases. Either the normal curvature will be a constant function of angle or it will attain a maximum and a minimum. The directions in which the extrema occur will be orthogonal. These directions are called the principal directions, and the curvatures are called the principal curvatures. The Gaussian curvature at a point is defined as the product of the principal curvatures. For example, the Gaussian curvature of the surface of a sphere of radius r is $1/r^2$. It can be shown[6] that the Gaussian curvature of a two-dimensional surface is related to the covariant curvature tensor by $K = R_{1212}/|g|$, where $|g|$ is the determinant of g_{ij} treated as a matrix.

REFERENCES AND NOTES

1. J. M. Pernter and F. M. Exner, *Meteorologische Optik*, 2nd ed. (Braumüller, Vienna, 1922).
2. S. Vince, "Observations upon an unusual horizontal refraction of the air; with remarks on the variations to which the lower parts of the atmosphere are sometimes subject," Philos. Trans. R. Soc. London **89,** 13–23 (1799).
3. W. H. Lehn and I. I. Schroeder, "Polar mirages as aids to Norse navigation," Polarforschung **49,** 173–187 (1979).
4. W. Kropla, "Obtaining temperature profiles from superior mirage data," master's thesis (University of Manitoba, Winnipeg, Manitoba, Canada, 1988).
5. R. K. Luneburg, *Mathematical Theory of Optics* (U. California Press, Berkeley, Calif., 1966).
6. D. Lovelock and H. Rund, *Tensors, Differential Forms, and Variational Principles* (Wiley, New York, 1975).
7. R. G. Fleagle and J. A. Businger, *An Introduction to Atmospheric Physics,* 2nd ed. (Academic, New York, 1980).
8. W. H. Lehn, "A simple parabolic model for the optics of the atmospheric surface layer," Appl. Math. Model. **9,** 447–453 (1985).
9. W. H. Lehn and M. B. El-Arini, "Computer-graphics analysis of atmospheric refraction," Appl. Opt. **17,** 3146–3151 (1978).
10. W. Tape, "The topology of mirages," Sci. Am. **252**(6), 120–129 (1985).
11. W. G. Rees, "Mirages with linear image diagrams," J. Opt. Soc. Am. A **7,** 1351–1354 (1990).
12. W. H. Lehn and B. A. German, "Novaya Zemlya effect: analysis of an observation," Appl. Opt. **20,** 2043–2047 (1981).
13. G. H. Liljequist, "Refraction phenomena in the polar atmosphere," in *Norwegian–British–Swedish Antarctic Expedition, 1949–52, Scientific Results* (Oslo U. Press, Oslo, Norway, 1964), Vol. 2, Part 2.
14. W. H. Lehn, "The Novaya Zemlya effect: an arctic mirage," J. Opt. Soc. Am. **69,** 776–781 (1979).
15. The elevation had previously been reported as 18.7 m. A survey conducted in 1983 indicated that the true elevation of Whitefish Summit is 20.3 m above sea level.
16. B. O'Neill, *Elementary Differential Geometry* (Academic, New York, 1966).